

Characterisation of irradiated thin silicon sensors for the CMS phase II pixel upgrade

The Tracker Group of the CMS Collaboration*

Corresponding authors:

Matteo Centis Vignali, Hamburg University, Luruper Chaussee 149, 22761 Hamburg, Germany

Thomas Eichhorn, Deutsches Elektronen-Synchrotron DESY, Notkestraße 85, 22607 Hamburg, Germany

Received: 19 May 2017 / Accepted: 27 July 2017 / Published online: 22 August 2017

© The Author(s) 2017. This article is an open access publication

Abstract The high luminosity upgrade of the Large Hadron Collider, foreseen for 2026, necessitates the replacement of the CMS experiment's silicon tracker. The innermost layer of the new pixel detector will be exposed to severe radiation, corresponding to a 1 MeV neutron equivalent fluence of up to $\Phi_{eq} = 2 \times 10^{16} \text{ cm}^{-2}$, and an ionising dose of $\approx 5 \text{ MGy}$ after an integrated luminosity of 3000 fb^{-1} . Thin, planar silicon sensors are good candidates for this application, since the degradation of the signal produced by traversing particles is less severe than for thicker devices. In this paper, the results obtained from the characterisation of 100 and 200 μm thick p-bulk pad diodes and strip sensors irradiated up to fluences of $\Phi_{eq} = 1.3 \times 10^{16} \text{ cm}^{-2}$ are shown.

1 Introduction

The search for new particles and interactions at hadron colliders requires the measurement of rare processes. As a consequence, the luminosity of the accelerators involved in this research must constantly be increased. The CERN Large Hadron Collider (LHC) and its injector chain will undergo a series of upgrades that will ultimately result in an instantaneous luminosity of $5 \times 10^{34} \text{ cm}^{-2} \text{ s}^{-1}$. The upgraded LHC, referred to as the High Luminosity LHC (HL-LHC), is expected to be operational in 2026 [1]. During the subsequent ten-year period, it is expected to deliver an integrated luminosity of 3000 fb^{-1} . By exploiting the design margins of the HL-LHC, a luminosity of $7.5 \times 10^{34} \text{ cm}^{-2} \text{ s}^{-1}$ could be achieved, resulting in an integrated luminosity of 4000 fb^{-1} [2].

The CMS detector measures the properties of the particles produced in LHC collisions [3]. Many of the current CMS detector systems are not designed to operate at the luminosities that will be provided by the HL-LHC. An upgrade

(known as the Phase II upgrade) is therefore necessary to maintain efficient data taking.

During the Phase II upgrade the CMS pixel detector will be replaced. The innermost radius of the new detector will be 30 mm. The pixel sensors placed at this radius will experience a bulk damage corresponding to a 1 MeV neutron equivalent fluence of up to $\Phi_{eq} = 2 \times 10^{16} \text{ cm}^{-2}$ and an ionising dose of approximately 5 MGy after an integrated luminosity of 3000 fb^{-1} [4].

The sensor types investigated by the CMS Collaboration for this pixel upgrade are 3D sensors and thin planar sensors with an active thickness between 75 and 200 μm [5]. Previous studies have shown that the degradation of the signal produced by traversing particles is less severe for thin sensors than for thicker devices [6–8].

This paper presents the results of the study of irradiated thin planar silicon sensors. In Sect. 2 the sensors and the irradiations used in this study are described. Section 3 contains the measurements performed using pad diodes and Sect. 4 those using strip sensors. Finally, the results obtained are summarised in Sect. 5.

2 Sensors and irradiations

The sensors used for this study were produced on oxygen rich silicon crystals (with a concentration of about $10^{17} \text{ atoms/cm}^3$) produced by epitaxial growth. The orientation of the crystal lattice is $\langle 100 \rangle$. The epitaxial silicon has a thickness of 100 μm and a resistivity of between 1 and 1.5 k $\Omega \text{ cm}$, determined using the capacitance-voltage characteristic of the sensors. The crystal is grown on a 220 μm thick substrate with a resistivity of $18 \times 10^{-3} \Omega \text{ cm}$ [9]. The difference in doping concentration between the epitaxial silicon and the growth substrate ensures that the charge collection volume of the sensors is restricted to the epitaxial silicon.

* e-mail: matteo.centis.vignali@cern.ch; thomas.eichhorn@desy.de

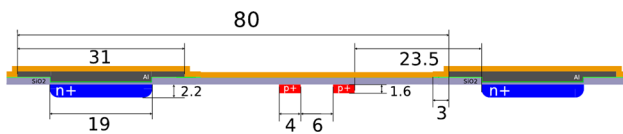


Fig. 1 Cross section of the surface design of a strip sensor with p-stop isolation. In the schematic it is possible to distinguish the n^+ strip implants and their metallisation, the p^+ p-stop implants, and the passivation layers. The distances are given in μm . The p-doped bulk and the ohmic contact on the back side are not shown [10]

The sensors realised on the substrate are pad diodes and strip detectors. The strips and pad diodes were each produced on both p- and n-doped silicon. The pad diodes are square with an area of $5 \times 5 \text{ mm}^2$. The metallisation on the junction side of the diodes has a $3 \times 3 \text{ mm}^2$ hole in the centre to allow laser light to be shone into the diodes. This can be used to study their charge collection efficiency. A guard ring surrounds the junction implant of the diodes. The diodes produced on a p-doped substrate have p-spray isolation between the junction and guard ring implants.

The strip sensors each have 64 strips with a pitch of $80 \mu\text{m}$. The strip implants are capacitatively coupled to the metallisation, which in turn is connected to the read-out electronics. The length of the strips is 25 mm , giving a total sensor area of $25 \times 5.12 \text{ mm}^2$. The implants are biased through a polysilicon resistor. The cross section of one such strip sensor is shown in Fig. 1. The strip sensors realised on a p-doped substrate have either p-spray or p-stop isolation. In the case of the p-stop isolation, every strip is enclosed by an individual p-stop implant.

The sensors were irradiated with 24 GeV/c protons (hardness factor¹ $\kappa = 0.62$) at the IRRAD [12] facility to fluences of $\Phi_{eq} = 1.5, 3$ and $13 \times 10^{15} \text{ cm}^{-2}$. Some strip sensors were irradiated with 800 MeV/c protons ($\kappa = 0.71$) at the LANSCE [13] facility to a fluence of $\Phi_{eq} = 1 \times 10^{15} \text{ cm}^{-2}$. No bias voltage or cooling was applied during the irradiation process.

In addition to the sensors mentioned above, strip sensors with a physical and active thickness of $200 \mu\text{m}$ were studied. These sensors were produced on silicon crystals grown using the float zone and magnetic Czochralski techniques. The orientation of the crystal lattice in this case is $\langle 100 \rangle$. Both the magnetic Czochralski and the float zone sensors have a resistivity between 3 and $4 \text{ k}\Omega \text{ cm}$. The oxygen concentration is about $10^{17} \text{ atoms/cm}^3$ for the float zone sensors and $10^{18} \text{ atoms/cm}^3$ for the magnetic Czochralski sensors. The design of the strip implants and of the metallisation of these sensors is identical to that of the detectors realised on

Table 1 Summary of the sensors used in this study and the fluences they accumulated. The Y and P denote a p-spray or p-stop isolated sensor, respectively

Sensor	$\Phi_{eq} [10^{15} \text{ cm}^{-2}]$				
	0	1 ^a	1.5 ^b	3 ^b	13 ^b
Epi $100 \mu\text{m}$ diode	Y	–	Y	Y	Y
Epi $100 \mu\text{m}$ strip	YP	YP	YP	P	YP
MCz $200 \mu\text{m}$ strip	–	–	–	–	YP
FZ $200 \mu\text{m}$ strip	–	–	–	–	Y

^a 800 MeV/c protons

^b 24 GeV/c protons

epitaxial silicon. The available samples of $200 \mu\text{m}$ thickness were irradiated with 24 GeV/c protons to a fluence of $\Phi_{eq} = 1.3 \times 10^{16} \text{ cm}^{-2}$.

A summary of the sensors used in this study together with the fluences they accumulated is given in Table 1. The different methods used to grow the silicon crystals are indicated as Epi, FZ and MCz for the epitaxial, float zone and magnetic Czochralski techniques, respectively. This convention is used throughout the remainder of this paper.

All the sensors were kept at a temperature of -18°C after irradiation in order to minimise annealing effects. Since no cooling was applied during the irradiation and the irradiation time varies with fluence, the sensors characterised in this study are in different annealing states.

3 Pad diode measurements

The diodes were characterised using laboratory measurements. The current–voltage characteristic and charge collection efficiency are presented below for p-bulk diodes.

3.1 Current–voltage characteristic

The current–voltage (IV) characteristic of the diodes was measured on a temperature controlled chuck. All the measurements were made at a temperature of 0°C . The guard ring surrounding the junction implant of the diode was set to the same potential as the junction implant to better define the volume of silicon contributing to the IV measurements. Examples of the IV characteristics of non-irradiated and irradiated diodes are shown in Figs. 2 and 3.

The IV characteristic of the non-irradiated diode does not saturate above full depletion voltage (around 80 V). This behaviour is thought to derive from the contribution of trap assisted tunnelling to the current [14]. The reduced thickness of the sensors results in an electric field high enough that the contribution to the current from electrons tunnelling from the valence to the conduction band becomes noticeable. The traps present due to imperfections in the crystal enhance the

¹ The hardness factor κ expresses the ratio between the fluence of the particles that traversed the sensor and the fluence of 1 MeV neutrons that produces the same non ionising energy loss (NIEL) with the relation $\Phi_{eq} = \kappa \Phi$ [11].

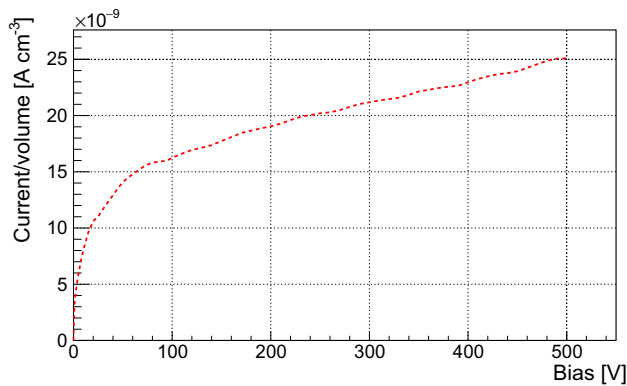


Fig. 2 IV characteristic of a non-irradiated p-bulk pad diode produced on epitaxial silicon measured at 0 °C. The current is normalised to the diode volume. The increase of the current above full depletion voltage (about 80 V) is ascribed to the contribution of trap assisted tunnelling to the current

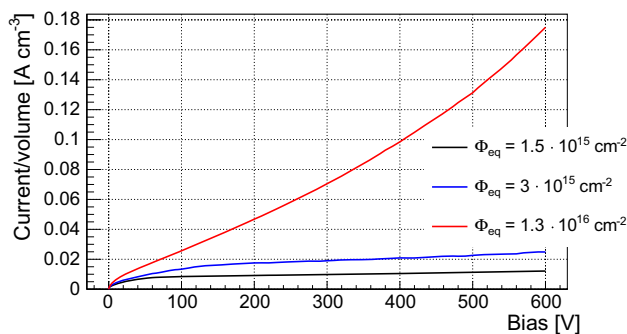


Fig. 3 IV characteristics of p-bulk pad diodes produced on epitaxial silicon irradiated to different fluences measured at 0 °C. The current is normalised to the diode volume

electron tunnelling rate. The imperfections originate during crystal growth and the production of the sensor.

3.2 Charge collection efficiency

The charge collection efficiency (CCE) of the diodes was measured by generating electron-hole pairs in the sensors using a pulsed infrared laser with a wavelength of 1060 nm. The absorption length of infrared light of this wavelength in silicon is bigger than the sensor thickness [15], resulting in the generation of electron-hole pairs in the whole sensor thickness. The signal induced in the sensor is amplified and subsequently digitised by an oscilloscope. The waveforms are averaged 512 times in the oscilloscope to reduce the effects of noise. The stability of the laser intensity is monitored by measuring the signal produced in non-irradiated diodes before and after each CCE measurement. The waveforms are integrated and the value obtained is used to estimate the CCE of the sensors. The results are normalised using the mean value of the integrated waveforms measured using non-irradiated sensors operated above full depletion voltage. The CCE of p-bulk diodes is shown in Fig. 4. The plot includes

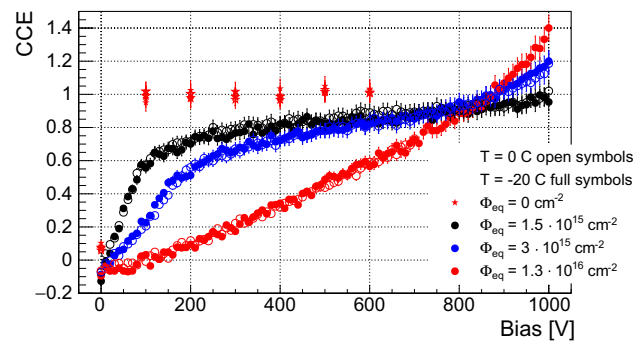


Fig. 4 Charge collection efficiency of p-bulk diodes before and after irradiation

measurements performed at 0 and −20 °C. The CCE of the pad diodes irradiated to 1.5 and $3 \times 10^{15} \text{ cm}^{-2}$ shows a kink around bias voltages of 100 and 200 V, respectively. The CCE of these sensors does not show any saturation after the kink. The diode subjected to a fluence of $1.3 \times 10^{16} \text{ cm}^{-2}$ also does not show such a kink in its CCE characteristic. These observations agree with the notion that full depletion voltage does not apply for devices that have accumulated such high fluences. The CCE exceeds unity at high bias voltages for diodes irradiated to 3 and $13 \times 10^{15} \text{ cm}^{-2}$. This effect can be interpreted as a manifestation of charge multiplication in the sensor. The effect has already been observed for devices and irradiations similar to the ones presented in this paper [16]. The contribution of charge multiplication to the current drawn by the sensors could provide an explanation for the shape of the IV characteristics shown in Fig. 3.

Another effect that could explain a CCE higher than unity would be an increase in the efficiency for the production of charge pairs by radiation-induced traps. Measurements of this effect are ongoing and suggest a reduction in the absorption length for the wavelength used in the measurements once the sensors have been irradiated [17]. This would result in a higher deposition of charge in irradiated sensors compared to the non-irradiated ones. This hypothesis is currently under investigation.

4 Strip sensor measurements

The strip sensors were characterised in a series of beam tests at the DESY II facility [18]. The aim of these beam tests was to measure the signal produced by a minimum ionising particle in the irradiated sensors. The signal is identified using the tracking information obtained from a beam telescope. The knowledge of the beam particles' impact position on the sensor improves the separation of signal and noise, allowing the analysis to be performed without it being necessary to apply any selection requirements on the signal.

The n-bulk sensors showed a very high noise, which is attributed to micro-discharges [10, 19]. Since the alignment

performed between the sensors and the beam telescope is done using the particle impact position measured by the strip sensors, the high level of noise resulted in the incorrect alignment of the n-bulk sensors with respect to the beam telescope. Therefore, the results presented in this section refer to the strip sensors with p-bulk only.

4.1 Beam test setup

The beam test measurements were performed at the DESY II facility using two beam lines. A monochromatic beam of electrons or positrons (depending on the beam line) with momentum between 3.5 and 5 GeV/c was used to characterise the sensors. The tracks of the beam particles were measured using either the Datura or the ACONITE pixel telescope [20,21]. The strip sensors were placed in a light-tight box where they could be cooled down to -28°C to reduce the leakage current. The non-irradiated sensors were measured at a temperature of 20°C , while the irradiated ones were measured at either -20 or -28°C . Three planes of the telescope were placed upstream of the light-tight box and three planes downstream. A fourfold coincidence of two pairs of scintillator plates defines the trigger for the setup. One pair of scintillator plates was placed upstream and the other downstream of the telescope planes. The signal from the strip sensors was read out using the ALiBaVa system [22].

A detailed description of the track reconstruction and alignment procedures used in the beam test is given in [19]. The signal processing, correction for temperature effects, and calibration of the analog to digital converter (ADC) used in the setup are described in [19,23].

4.2 Signal extraction

In order to determine the total signal induced on the sensor's strips, it is necessary to define a clustering criterion. The cluster charge is defined as the sum of the charges induced on a group of five adjacent strips, which is centred on the strip that is traversed by a particle. The strips that are traversed by a particle are identified using the tracking information provided by the telescope. This cluster definition has the advantage of avoiding the application of any requirements on the signal induced in the strips. This minimises the bias on the charge spectra caused by the cluster selection. The advantages of this method are summarised in [24].

The 5-strip cluster charge distribution obtained for a $100\text{ }\mu\text{m}$ thick sensor irradiated to $\Phi_{eq} = 1.3 \times 10^{16}\text{ cm}^{-2}$ and biased to 800 V, together with the results of the fit used to describe the distribution, is shown in Fig. 5. A similar distribution was measured for each sensor at each bias step. The fit function is the sum of a Gaussian distribution and a Landau–Gauss convolution function.

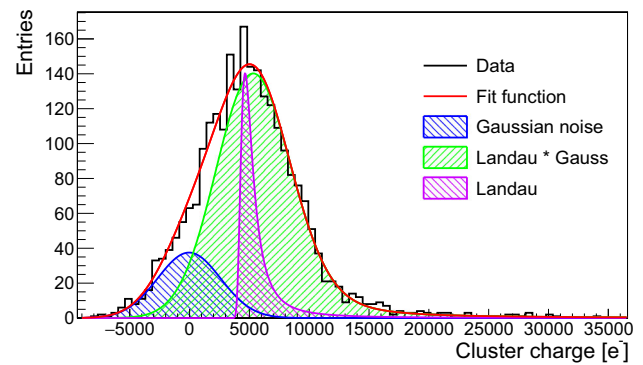


Fig. 5 5-strip cluster charge distribution for a p-bulk strip sensor with $100\text{ }\mu\text{m}$ active thickness, irradiated to $\Phi_{eq} = 1.3 \times 10^{16}\text{ cm}^{-2}$ and biased to 800 V. The different components of the function used to describe the distribution are shown

The Landau–Gauss convolution function accounts for the energy loss in the sensor and the noise in the sensor and electronics. The implementation of the Landau distribution and the code used for the Landau–Gauss convolution are described in [25,26], respectively.

The Gaussian distribution centred around zero describes the contribution of events that are not correctly reconstructed. Since the sampling time of the telescope is longer than that of the ALiBaVa setup ($115\text{ }\mu\text{s}$ and 25 ns , respectively), the telescope can register more tracks than the strip sensor in any given event. The timing information for the tracks within one event is not available. The coincidence of the trigger scintillators assures that at least one particle traverses the setup at the time of the ALiBaVa read-out. Selection requirements are applied to find the track corresponding to this particle. If the track associated with the particle that triggered the read-out is not reconstructed in the beam telescope, a different track is selected. The selected track can point to a group of strips on the sensor that were not traversed by a particle during the ALiBaVa read-out, resulting in a cluster where no signal is present. The charge distribution of the events where the track of the particle triggering the read-out is not reconstructed is identical to the noise for a group of five strips. The mean and standard deviation of the Gaussian centred around zero can therefore be determined from the noise measurements of the sensors (c.f. Sect. 4.3) and are therefore not considered to be free parameters in the fit to the 5-strip cluster charge distribution.

The parameters optimised in the fit of the 5-strip charge distribution are:

- The area of the Gaussian centred around zero.
- The width parameter of the Landau distribution.
- The most probable value (MPV) of the Landau distribution.
- The area of the Landau–Gauss convolution.
- The standard deviation of the Gaussian used in the convolution.

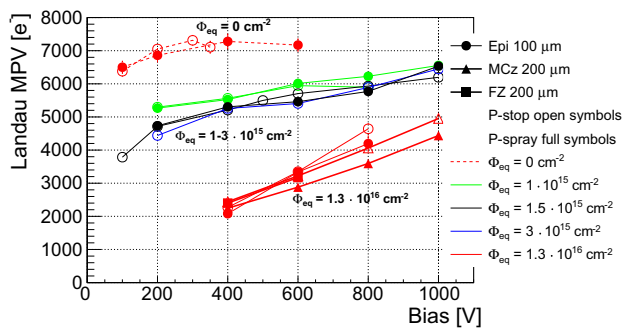


Fig. 6 Most probable value of the Landau component of the distribution fitted to the cluster charge distribution for different p-bulk sensors as a function of fluence and bias voltage. The measurements shown here were performed with the beam traversing the sensors at normal incidence. The MPV of the float zone sensor irradiated to $\Phi_{eq} = 1.3 \times 10^{16} \text{ cm}^{-2}$ measured at 400 and 600 V bias is very similar to those observed for magnetic Czochralski and epitaxial sensors irradiated to the same fluence

The full range of the distribution is used in the fit. The parameter optimisation is performed using the Log Likelihood method implemented in ROOT [27].

The MPV of the Landau distribution is used to compare the different sensors.

Figure 6 shows the Landau MPV of the p-bulk sensors measured in the beam test as a function of bias voltage and fluence. The beam incidence was normal to the sensors. The error bars include a statistical contribution from the fit as well as systematic uncertainties arising from the conversion from ADC counts into electrons. The non-irradiated 100 μm thick sensors show MPV values around 7000 e^- . The 100 μm thick sensors irradiated between 1 and $3 \times 10^{15} \text{ cm}^{-2}$ show similar values for the collected charge. This could be the result of the different annealing states of the sensors due to the different amounts of time necessary to accumulate the fluence during irradiation. An improvement in the charge collection after annealing was observed for thin sensors produced on float zone silicon [28]. The 100 μm thick sensors irradiated to $1.3 \times 10^{16} \text{ cm}^{-2}$ show a signal between 4000 and 5000 electrons at a bias voltage of 800 V. The 200 μm thick sensors show a similar value for the signal, at a bias voltage that is about 200 V higher.

The values of charge collected by the 100 and 200 μm thick sensors irradiated to $\Phi_{eq} = 1.3 \times 10^{16} \text{ cm}^{-2}$ are similar to the ones reported in [6] for strip sensors irradiated with neutrons to $\Phi_{eq} = 2 \times 10^{16} \text{ cm}^{-2}$. The results obtained with the 200 μm thick float zone sensor irradiated to $\Phi_{eq} = 1.3 \times 10^{16} \text{ cm}^{-2}$ are consistent with the ones reported in [28] measured using pixel sensors irradiated with protons to $\Phi_{eq} = 1.4 \times 10^{16} \text{ cm}^{-2}$.

In the range of fluences and bias voltages considered in this study, the values for the signal obtained from p-spray and p-stop isolated sensors are very similar.

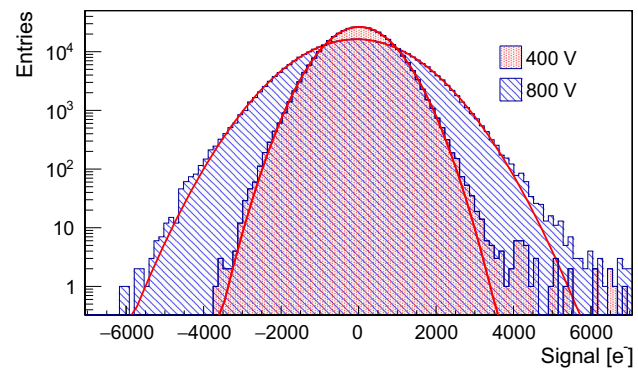


Fig. 7 Noise distribution for a single channel of a 100 μm thick p-bulk sensor irradiated to $\Phi_{eq} = 1.3 \times 10^{16} \text{ cm}^{-2}$ and biased to 400 and 800 V. The red lines represent the result of Gaussian fits to the data

4.3 Noise measurements

The sensors' and read-out electronics' noise was determined using the data collected during the beam test. The tracking information provided by the beam telescope was used to exclude the strips traversed by particles from the noise estimation. Figure 7 shows the noise distribution for a single channel for a 100 μm thick sensor, irradiated to $\Phi_{eq} = 1.3 \times 10^{16} \text{ cm}^{-2}$, and biased to 400 and 800 V. The distributions are similar to Gaussians, represented by the red lines in the figure. The tail present on the right hand side of each distribution is caused by particles from tracks that were not correctly reconstructed. Micro-discharges do not affect the noise distribution for p-bulk sensors. The noise distribution for irradiated n-bulk sensors shows non-Gaussian tails on both sides and a strong dependence of the number of entries in the tails on the bias voltage [10, 19]. A Gaussian fit is used to extract the standard deviation (σ) of the noise distribution. In order to avoid the influence of the tail on the extracted parameters, the range of the fit was chosen to be from $\mu - 3\sigma$ to $\mu + 2\sigma$, where μ represents the mean of the distribution.

The value of σ averaged over the channels is shown in Fig. 8 as a function of fluence and bias voltage for different sensors. The standard deviation of the noise distribution lies at around 750 e^- for the 100 μm thick non-irradiated sensors. The 100 μm thick sensors irradiated to $\Phi_{eq} \leq 3 \times 10^{15} \text{ cm}^{-2}$ show a similar value for bias voltages below 600 V. The irradiated sensors show a noise comparable to that observed for the non-irradiated sensors despite the larger dark current that results in a larger shot noise. The shot noise contribution for this range of bias and fluence was estimated from the sensors' dark current to be less than 300 e^- . The sensors irradiated to $\Phi_{eq} = 1.3 \times 10^{16} \text{ cm}^{-2}$ show a different behaviour, depending on their thickness. The 100 μm thick sensors show a steep increase in noise between 600 and 800 V. The 200 μm thick sensors show a lower noise than the 100 μm thick sensors.

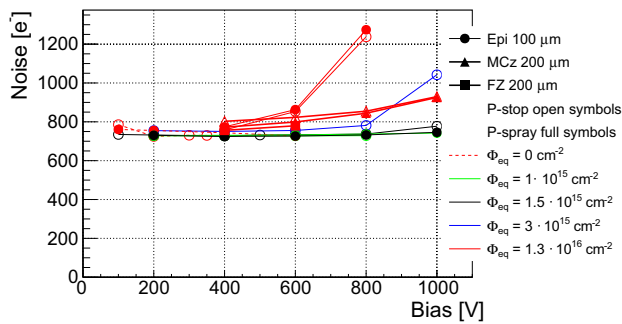


Fig. 8 Mean value of the standard deviation of the single channel noise distribution for p-bulk sensors as a function of fluence and bias voltage

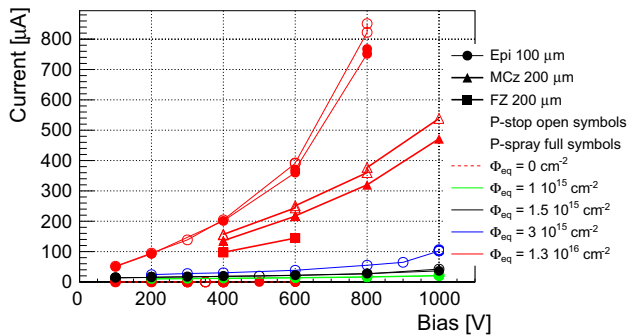


Fig. 9 Current–voltage characteristic of the p-bulk strip sensors as measured during the beam test. The current values are scaled to a sensor temperature of -20°C

It should be stressed that the single channel noise expected from a future irradiated pixel detector is significantly lower than the one shown in Fig. 8 for irradiated strip sensors. The smaller channel dimension of a pixel sensor results in a smaller silicon volume contributing to the leakage current and to a smaller capacitance.

The IV characteristic of the strip sensors, shown in Fig. 9, contributes to the understanding of the behaviour of the sensors' noise. The IV characteristics were measured at the beam test facility when the particle beam was not traversing the sensors. The current values were scaled to a sensor temperature of -20°C using the usual expression derived in [29]. The resulting scaling factor is 2.64 for the sensors irradiated to $\Phi_{eq} = 1.3 \times 10^{16} \text{ cm}^{-2}$ and measured at -28°C .

The $100 \mu\text{m}$ thick sensors irradiated to $\Phi_{eq} = 1.3 \times 10^{16} \text{ cm}^{-2}$, despite having a smaller volume, draw more current than the $200 \mu\text{m}$ thick ones. This could explain the behaviour observed in their corresponding noise distribution.

The mechanism responsible for the high current values, observed in the highly irradiated $100 \mu\text{m}$ thick strip sensors at high bias voltages, is consistent with charge multiplication. This effect explains the observed increase of current, signal, and noise as a function of the bias voltage. This result is consistent with the observation by other groups of charge multiplication in irradiated strip sensors [30].

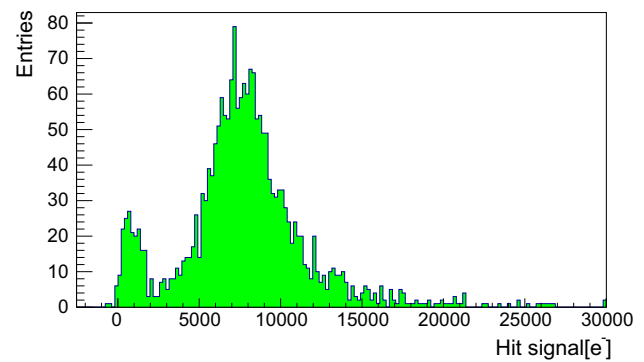


Fig. 10 Seed strip charge distribution for a non-irradiated p-bulk sensor, biased to 300 V

4.4 Detection efficiency

The pixel detectors used at high luminosity hadron colliders implement a zero suppression of data at an early stage of the read-out chain in order to reduce the data bandwidth of the detector system. This is usually achieved by setting a threshold on the read-out channel for each individual pixel. The degradation of the sensor signal with radiation damage can therefore influence the detection efficiency.

The detection efficiency of the strip sensors was studied using the charge collected by the seed strip of the 5-strip clusters. The seed strip is defined to be the strip with the highest signal in the cluster. The seed strip charge distribution for a non-irradiated sensor is shown in Fig. 10. The distribution has two components: a noise peak close to zero and the signal produced by ionising particles at higher values. The noise peak present in this distribution originates from the mechanism described in Sect. 4.2. The shape of the noise peak is, however, no longer Gaussian as the seed strip is the one with the highest signal in the cluster. In this case the shape can be derived by considering the probability of a strip having a signal x , at the same time as the others all having smaller signals. For clusters with n strips, this probability is given by:

$$P_n(x, \sigma) = nN(x, \sigma) \left(\int_{-\infty}^x N(y, \sigma) dy \right)^{n-1}$$

where σ is the standard deviation of the single channel noise distribution, and $N(x, \sigma)$ is the normal distribution that describes the single channel noise.

In the analysis of the seed strip charge distribution, the noise peak was subtracted from the distribution. The noise distribution is estimated by clustering the strips in groups of five and selecting the highest signal when the strips are not traversed by a particle. The noise distribution obtained in this way is scaled and subtracted from the seed strip charge distribution. Figure 11 shows the seed strip charge distribution of a

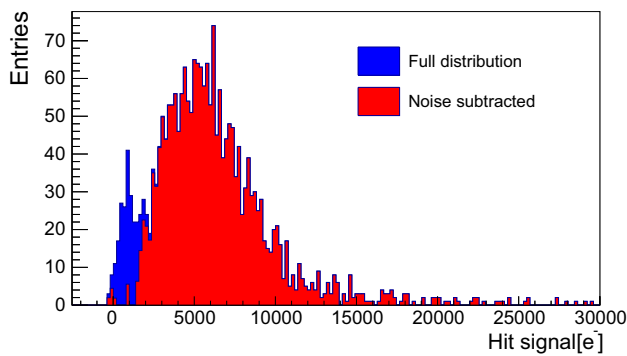


Fig. 11 Seed strip charge distribution for a p-bulk sensor irradiated to $\Phi_{eq} = 3 \times 10^{15} \text{ cm}^{-2}$ and biased to 800 V. The distribution is shown before and after noise peak subtraction

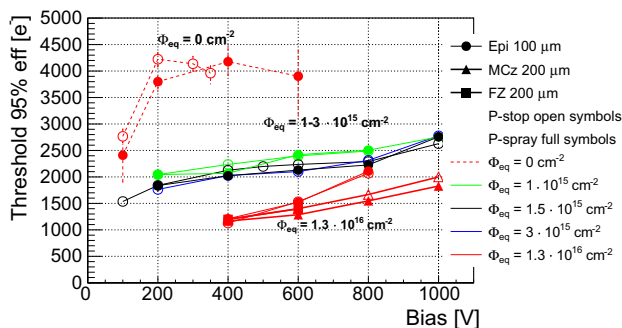


Fig. 12 Threshold corresponding to 95% detection efficiency for p-bulk sensors as a function of fluence and bias voltage

100 μm thick sensor irradiated to $\Phi_{eq} = 3 \times 10^{15} \text{ cm}^{-2}$ and biased to 800 V before and after the noise peak is subtracted.

To determine the effect of a pulse height threshold on the detection efficiency, a target detection efficiency of 95% was chosen and the corresponding threshold derived from the seed strip charge distribution. The statistical sample contained in the distributions used for this analysis is around 1500 events after noise peak subtraction. In order to perform the same analysis with higher target efficiencies (e.g. 99%), a larger sample would be needed. The threshold corresponding to 95% detection efficiency is shown as a function of fluence and bias voltage in Fig. 12.

The threshold values found for the non-irradiated sensors lie at around 4000 e^- . The 100 μm thick sensors irradiated from 1 to $3 \times 10^{15} \text{ cm}^{-2}$ require a threshold of around 2500 e^- . Finally for the sensors irradiated to $\Phi_{eq} = 1.3 \times 10^{16} \text{ cm}^{-2}$ a threshold of about 2000 e^- is found, regardless of the sensors' thickness. These values can be compared to the threshold of approximately 1500 e^- achieved by the read-out chip used in the CMS Phase I pixel upgrade [31]. The design threshold of the read-out chip for the Phase II pixel upgrade is about 1000 e^- [32].

The reduction of the threshold required to maintain a certain efficiency after irradiation is the consequence of two

effects. First, the amount of collected charge decreases with the accumulated fluence. Second, the shape of the seed strip charge distribution is affected by irradiation, as can be seen in Figs. 10 and 11. The latter effect is the consequence of charge sharing between strips being enhanced by irradiation. This is explained in more detail in [19,23]. A similar effect was observed for strip sensors irradiated with low energy electrons, which was ascribed to the influence of the build-up of charge in the sensor passivation on the sensor electric field [33].

5 Summary

The CMS Phase II pixel upgrade foreseen for 2026 requires the development of silicon sensors able to withstand a fluence of $\Phi_{eq} = 2 \times 10^{16} \text{ cm}^{-2}$.

The results of the characterisation of p-bulk silicon diodes and strip sensors with an active thickness of 100 and 200 μm , irradiated up to $\Phi_{eq} = 1.3 \times 10^{16} \text{ cm}^{-2}$, are presented in this paper. Charge multiplication was observed in 100 μm thick pad diodes and strip sensors irradiated to $\Phi_{eq} = 1.3 \times 10^{16} \text{ cm}^{-2}$ with an applied bias voltage of 800 V. The signal produced by minimum ionising particles in the strip sensors lies between 4000 and 5000 e^- for both the 100 and 200 μm thick sensors after irradiation at the highest fluences used. The threshold required to maintain 95% detection efficiency is found to be around 2000 e^- for both 100 and 200 μm thick sensors after being irradiated to $\Phi_{eq} = 1.3 \times 10^{16} \text{ cm}^{-2}$. The bias voltage applied to the sensors was 800 and 1000 V, respectively.

This performance shows that thin silicon sensors produced using the planar process are good sensor candidates for the outer layers of the pixel detector for the CMS Phase II pixel upgrade. The employment of these sensors for the innermost layer of the upgraded pixel detector has to be studied, although the performance shown so far is encouraging.

As the measurements do not show a clear difference between p-spray and p-stop isolated sensors, no conclusion regarding this design choice can be drawn.

The performance of the thin sensors presented in this paper must be corroborated by measurements performed using pixel sensors. The difference in the electric and weighting fields between pixel and strip sensors could result in a different performance between the two.

Acknowledgements The authors wish to thank the shifters of the test beam campaign, the students that performed the measurements on diodes, and E. Yildirim for support in the use of the read-out system. The research leading to these results has received funding from the European Commission under the FP7 Research Infrastructures project AIDA, Grant agreement no. 262025 and the PIER Ideenfonds PIF-2013-23.

Open Access This article is distributed under the terms of the Creative Commons Attribution 4.0 International License (<http://creativecommons.org/licenses/by/4.0/>), which permits unrestricted use, distribution, and reproduction in any medium, provided you give appropriate credit to the original author(s) and the source, provide a link to the Creative Commons license, and indicate if changes were made. Funded by SCOAP³.

References

- HiLumi LHC Collaboration, Preliminary Design Report (2014). <http://hilumilhc.web.cern.ch/science/deliverables>
- L. Rossi, Introduction to the HL-LHC Project (2017). <https://indico.cern.ch/event/606369/>
- CMS Collaboration, The CMS experiment at the CERN LHC. JINST **3**(S08004) (2008). doi:10.1088/1748-0221/3/08/S08004
- CMS Collaboration, FLUKA particle flux maps for CMS Detector (2013). <https://cds.cern.ch/record/1612355>
- G. Steinbrück, Small pitch pixel sensors for the CMS Phase II upgrade (2015). <https://cds.cern.ch/record/2108949>
- G. Casse et al., Thin silicon detectors for tracking in high radiation environments, in *IEEE Proceedings NSS/MIC*, pp. 1661–1663 (2012). doi:10.1109/NSSMIC.2012.6551394
- S. Kuehn on behalf of the RD50 collaboration, Development of new radiation hard detectors. Nucl. Instr. Meth. Phys. Res. A **824**, 422 (2016). doi:10.1016/j.nima.2015.09.107
- S. Terzo et al., Heavily irradiated N-in-p thin planar pixel sensors with and without active edges. JINST **9**(05), C05023 (2014). doi:10.1088/1748-0221/9/05/C05023
- A. Dierlamm, Private communication
- J. Erfle, Irradiation study of different silicon materials for the CMS tracker upgrade. Ph.D. thesis, Hamburg University. DESY-THESIS-2014-010 (2014)
- M. Moll, Radiation damage in silicon particle detectors. Ph.D. thesis, Hamburg University. DESY-THESIS-1999-040 (1999)
- <http://ps-irrad.web.cern.ch/>. Accessed 14 Aug 2017
- <http://lansce.lanl.gov/>. Accessed 14 Aug 2017
- G. Hurkx, D. Klaassen, M. Knuvers, A new recombination model for device simulation including tunneling. IEEE Trans. Electron Devices **39**(2), 331 (1992). doi:10.1109/16.121690
- M.A. Green, Self-consistent optical parameters of intrinsic silicon at 300 K including temperature coefficients Sol. Energy Mater. Sol. Cells **92**, 1305–1310 (2008). doi:10.1016/j.solmat.2008.06.009
- J. Lange et al., Properties of a radiation-induced charge multiplication region in epitaxial silicon diodes. Nucl. Instr. Meth. Phys. Res. A, **622**(1): 49–58 (2010). doi:10.1016/j.nima.2010.07.036
- C. Scharf, Private communication
- <http://testbeam.desy.de/>. Accessed 14 Aug 2017
- T. Eichhorn, Development of Silicon Detectors for the High Luminosity LHC. Ph.D. thesis, Hamburg University. DESY-THESIS-2015-024 (2015)
- <https://telescopes.desy.de/>. Accessed 14 Aug 2017
- H. Jansen et al., Performance of the EUDET-type beam telescopes EPJ Tech. Instrum. **3**(1) (2016). doi:10.1140/epjti/s40485-016-0033-2
- R. Marco-Hernandez, A portable readout system for microstrip silicon sensors (ALIBAVA). IEEE. Trans. Nucl. Sci. **56**(3), 1642 (2009). doi:10.1109/TNS.2009.2017261
- M. Centis Vignali, Silicon Sensors for the Upgrades of the CMS Pixel Detector. Ph.D. thesis, Hamburg University. DESY-THESIS-2015-052 (2015)
- T. Mäenpää, M. Kortelainen, T. Lampen, Track-induced clustering in position sensitive detector characterization, in *IEEE Proceedings NSS/MIC*, pp. 832–835 (2009). doi:10.1109/NSSMIC.2009.5402394
- K.S. Kölbig, B. Schorr, A program package for the Landau distribution. Comput. Phys. Commun. **31**, 97 (1984). doi:10.1016/0010-4655(84)90085-7
- H. Pernegger, M. Friedl, Convolved Landau and Gaussian fitting function (using ROOT's Landau and Gauss functions). <https://root.cern.ch/root/html/tutorials/fit/langaus.C.html>. Accessed 14 Aug 2017
- <http://root.cern.ch>. Accessed 14 Aug 2017
- S. Terzo et al., Thin n-in-p planar pixel sensors and active edge sensors for the ATLAS upgrade at HL-LHC. JINST **9**(12), C12029 (2014). doi:10.1088/1748-0221/9/12/C12029
- A. Chilingarov, Generation current temperature scaling. (2013). <http://cds.cern.ch/record/1511886>
- G. Casse on behalf of the RD50 collaboration, The RD50 activity in the context of future pixel detector systems. JINST **10**(05), C05020 (2014). doi:10.1088/1748-0221/10/05/C05020
- S. Spannagel, Test beam campaigns for the CMS phase I upgrade pixel readout chip. JINST **9**(12), C12001 (2014). doi:10.1088/1748-0221/9/12/C12001
- M. Garcia-Sciveres, RD53A integrated circuit specifications (2015). <https://cds.cern.ch/record/2113263>
- The Tracker Group of the CMS Collaboration, Impact of low-dose electron irradiation on n+p silicon strip sensor. Nucl. Instr. Meth. Phys. Res. A **803**(1): 100–112 (2015). doi:10.1016/j.nima.2015.08.026

The Tracker Group of the CMS Collaboration

Institut für Hochenergiephysik, Vienna, Austria

W. Adam, T. Bergauer, E. Brondolin, M. Dragicevic, M. Friedl, R. Frühwirth¹, M. Hoch, J. Hrubec, A. König, H. Steininger, W. Waltenberger

Universiteit Antwerpen, Antwerp, Belgium

S. Alderweireldt, W. Beaumont, X. Janssen, J. Lauwers, P. Van Mechelen, N. Van Remortel, A. Van Spilbeeck

Université Libre de Bruxelles, Brussels, Belgium

D. Beghin, H. Brun, B. Clerbaux, H. Delannoy, G. De Lentdecker, G. Fasanella, L. Favart, R. Goldouzian, A. Grebenyuk, G. Karapostoli, Th. Lenzi, A. Léonard, J. Luetic, N. Postiau, T. Seva, P. Vanlaer, D. Vannerom, Q. Wang, F. Zhang

Vrije Universiteit Brussel, Brussels, Belgium

S. Abu Zeid, F. Blekman, I. De Bruyn, J. De Clercq, J. D'Hondt, K. Deroover, S. Lowette, S. Moortgat, L. Moreels, Q. Python, K. Skovpen, P. Van Mulders, I. Van Parijs

Université Catholique de Louvain, Louvain-la-Neuve, Belgium

H. Bakhshiansohi, O. Bondu, S. Brochet, G. Bruno, A. Caudron, C. Delaere, M. Delcourt, S. De Visscher, B. Francois, A. Giammanco, A. Jafari, M. Komm, G. Krintiras, V. Lemaître, A. Magitteri, A. Mertens, D. Michotte, M. Musich, K. Piotrkowski, L. Quertenmont, N. Szilasi, M. Vidal Marono, S. Wertz

Université de Mons, Mons, Belgium

N. Bely, T. Caebergs, E. Daubie, G. H. Hammad

Helsinki Institute of Physics, Helsinki, Finland

J. Härkönen, T. Lampén, P. Luukka, T. Peltola, E. Tuominen, E. Tuovinen

Department of Physics, University of Helsinki, Helsinki, Finland

P. Eerola

Lappeenranta University of Technology, Lappeenranta, Finland

T. Tuuva

Université de Lyon, Université Claude Bernard Lyon 1, CNRS-IN2P3, Institut de Physique Nucléaire de Lyon, Villeurbanne, France

G. Baulieu, G. Boudoul, L. Caponetto, C. Combaret, D. Contardo, T. Dupasquier, G. Gallbit, N. Lumb, L. Mirabito, S. Perries, M. Vander Donckt, S. Viret

Université de Strasbourg, CNRS, IPHC UMR, 7178 Strasbourg, France

J.-L. Agram², J. Andrea, D. Bloch, C. Bonnin, J.-M. Brom, E. Chabert, N. Chanon, L. Charles, E. Conte², J.-Ch. Fontaine², L. Gross, J. Hosselet, M. Jansova, D. Tromson

RWTH Aachen University, I. Physikalisches Institut, Aachen, Germany

C. Autermann, L. Feld, W. Karpinski, K. M. Kiesel, K. Klein, M. Lipinski, A. Ostapchuk, G. Pierschel, M. Preuten, M. Rauch, S. Schael, C. Schomakers, J. Schulz, G. Schwering, M. Wlochal, V. Zhukov

RWTH Aachen University, III. Physikalisches Institut B, Aachen, Germany

C. Pistone, G. Fluegge, A. Kuensken, O. Pooth, A. Stahl

Deutsches Elektronen-Synchrotron DESY, Notkestraße 85, 22607 Hamburg, Germany

M. Aldaya, C. Asawatangtrakuldee, K. Beernaert, D. Bertsche, C. Contreras-Campana, G. Eckerlin, D. Eckstein, T. Eichhorn, E. Gallo, J. Garay Garcia, K. Hansen, M. Haranko, A. Harb, J. Hauk, J. Keaveney, A. Kalogeropoulos, C. Kleinwort, W. Lohmann³, R. Mankel, H. Maser, G. Mittag, C. Muhl, A. Mussgiller, H. Perrey, D. Pitzl, O. Reichelt, M. Savitskyi, P. Schuetze, S. Spannagel, R. Walsh, A. Zuber

Hamburg University, Luruper Chaussee 149, 22761 Hamburg, Germany

H. Biskop, P. Buhmann, M. Centis-Vignali, E. Garutti, J. Haller, M. Hoffmann, A. Junkes, R. Klanner, T. Lapsien, M. Matysek, A. Perieanu, Ch. Scharf, P. Schleper, A. Schmidt, J. Schwandt, J. Sonneveld, G. Steinbrück, B. Vormwald, J. Wellhausen

Institut für Experimentelle Kernphysik, Karlsruhe, Germany

M. Abbas, C. Amstutz, T. Barvich, Ch. Barth, F. Boegelspacher, W. De Boer, E. Butz, M. Casele, F. Colombo, A. Dierlamm, B. Freund, F. Hartmann, S. Heindl, U. Husemann, A. Kornmeyer, S. Kudella, Th. Muller, H. J. Simonis, P. Steck, M. Weber, Th. Weiler

Institute of Nuclear and Particle Physics (INPP), NCSR Demokritos, Aghia Paraskevi, Greece

G. Anagnostou, P. Asenov, P. Assiouras, G. Daskalakis, A. Kyriakis, D. Loukas, L. Paspalaki

Wigner Research Centre for Physics, Budapest, Hungary

F. Siklér, V. Veszprémi

University of Delhi, Delhi, India

A. Bhardwaj, R. Dalal, G. Jain, K. Ranjan

Institute for Research in Fundamental Sciences (IPM), Tehran, Iran

H. Bakhshiansohl, H. Behnamian, M. Khakzad, M. Naseri

INFN Sezione di Bari^a, Università di Bari^b, Politecnico di Bari^c, Bari, Italy

P. Cariola^a, D. Creanza^{a,c}, M. De Palma^{a,b}, G. De Robertis^a, L. Fiore^a, M. Franco^a, F. Loddo^a, G. Sala^a, L. Silvestris^a, G. Maggi^{a,c}, S. My^{a,b}, G. Selvaggi^{a,b}

INFN Sezione di Catania^a, Università di Catania^b, Catania, Italy

S. Albergo^{a,b}, G. Cappello^{a,b}, M. Chiorboli^{a,b}, S. Costa^{a,b}, A. Di Mattia^a, F. Giordano^{a,b}, R. Potenza^{a,b}, M. A. Saizu^{a,4}, A. Tricomi^{a,b}, C. Tuve^{a,b}

INFN Sezione di Firenze^a, Università di Firenze^b, Florence, Italy

G. Barbagli^a, M. Brianzi^a, R. Ciaranfi^a, V. Ciulli^{a,b}, C. Civinini^a, R. D'Alessandro^{a,b}, E. Focardi^{a,b}, G. Latino^{a,b}, P. Lenzi^{a,b}, M. Meschini^a, S. Paoletti^a, L. Russo^{a,b}, E. Scarlini^{a,b}, G. Sguazzoni^a, D. Strom^a, L. Viliani^{a,b}

INFN Sezione di Genova^a, Università di Genova^b, Genoa, Italy

F. Ferro^a, M. Lo Vetere^{a,b}, E. Robutti^a

INFN Sezione di Milano-Bicocca^a, Università di Milano-Bicocca^b, Milan, Italy

M. E. Dinardo^{a,b}, S. Fiorendi^{a,b}, S. Gennai^a, S. Malvezzi^a, R. A. Manzoni^{a,b}, D. Menasce^a, L. Moroni^a, D. Pedrini^a

INFN Sezione di Padova^a, Università di Padova^b, Padua, Italy

P. Azzi^a, N. Bacchetta^a, D. Bisello^a, M. Dall'Osso^{a,b}, N. Pozzobon^{a,b}, M. Tosi^{a,b}

INFN Sezione di Pavia^a, Università di Bergamo^b, Bergamo, Italy

F. De Canio^{a,b}, L. Gaioni^{a,b}, M. Manghisoni^{a,b}, B. Nodari^{a,b}, E. Riciputi^{a,b}, V. Re^{a,b}, G. Traversi^{a,b}

INFN Sezione di Pavia^a, Università di Pavia^b, Pavia, Italy

D. Comotti^{a,b}, L. Ratti^{a,b}

INFN Sezione di Perugia^a, Università di Perugia^b, Perugia, Italy

L. Alunni Solestizi^{a,b}, M. Biasini^{a,b}, G. M. Bilei^a, C. Cecchi^{a,b}, B. Checcucci^a, D. Ciangottini^{a,b}, L. Fanò^{a,b}, C. Gentsos^a, M. Ionica^a, R. Leonardi^{a,b}, E. Manoni^{a,b}, G. Mantovani^{a,b}, S. Marconi^{a,b}, V. Mariani^{a,b}, M. Menichelli^a, A. Modak^{a,b}, A. Morozzi^{a,b}, F. Moscatelli^a, D. Passeri^{a,b}, P. Placidi^{a,b}, V. Postolache^a, A. Rossi^{a,b}, A. Saha^a, A. Santocchia^{a,b}, L. Storch^a, D. Spiga^a

INFN Sezione di Pisa^a, Università di Pisa^b, Scuola Normale Superiore di Pisa^c, Pisa, Italy

K. Androsov^a, P. Azzurri^a, S. Arezzini^a, G. Bagliesi^a, A. Basti^a, T. Boccali^a, L. Borrello^a, F. Bosi^a, R. Castaldi^a, A. Ciampa^a, M. A. Ciocci^{a,b}, R. Dell'Orso^a, S. Donato^{a,c}, G. Fedi^a, A. Giassi^a, M. T. Grippo^{a,5}, F. Ligabue^{a,c}, T. Lomtadze^a, G. Magazzu^a, L. Martini^{a,b}, E. Mazzoni^a, A. Messineo^{a,b}, A. Moggi^a, F. Morsani^a, F. Palla^a, F. Palmonari^a, F. Raffaelli^a, A. Rizzi^{a,b}, A. Savoy-Navarro^{a,6}, P. Spagnolo^a, R. Tenchini^a, G. Tonelli^{a,b}, A. Venturi^a, P. G. Verdini^a

INFN Sezione di Torino^a, Università di Torino^b, Turin, Italy

R. Bellan^{a,b}, M. Costa^{a,b}, R. Covarelli^{a,b}, M. Da Rocha Rolo^a, N. Demaria^a, A. Rivetti^a, G. Dellacasa^a, G. Mazza^a, E. Migliore^{a,b}, E. Monteil^{a,b}, L. Pacher^a, F. Ravera^{a,b}, A. Solano^{a,b}

Instituto de Física de Cantabria (IFCA), CSIC-Universidad de Cantabria, Santander, Spain

M. Fernandez, G. Gomez, R. Jaramillo Echeverria, D. Moya, F. J. Gonzalez Sanchez, I. Vila, A. L. Virto

CERN, European Organization for Nuclear Research, Geneva, Switzerland

D. Abbaneo, I. Ahmed, E. Albert, G. Auzinger, G. Berruti, G. Bianchi, G. Blanchot, J. Bonnaud, A. Caratelli, D. Ceresa, J. Christiansen, K. Cichy, J. Daguin, A. D'Auria, S. Detraz, D. Deyrail, O. Dondelewski, F. Faccio, N. Frank, T. Gadek, K. Gill, A. Honma, G. Hugo, L. M. Jara Casas, J. Kaplon, A. Kornmayer, L. Kottelat, M. Kovacs, M. Krammer¹, P. Lenoir, M. Mannelli, A. Marchioro, S. Marconi, S. Mersi, S. Martina, S. Michelis, M. Moll, A. Onnela, S. Orfanelli, S. Pavis, A. Peisert, J.-F. Pernot, P. Petagna, G. Petrucciani, H. Postema, P. Rose, P. Tropea, J. Troska, A. Tsirou, F. Vasey, P. Vichoudis, B. Verlaat, L. Zwalinski

Institute for Particle Physics ETH Zurich, Zurich, Switzerland

F. Bachmair, R. Becker, D. di Calafiori, B. Casal, P. Berger, L. Djambazov, M. Donega, C. Grab, D. Hits, J. Hoss, G. Kasieczka, W. Lustermann, B. Mangano, M. Marionneau, P. Martinez Ruiz del Arbol, M. Masciovecchio, M. Meinhard, L. Perozzi, U. Roeser, A. Starodumov⁷, V. Tavoraro, R. Wallny, D. Zhu

Universität Zürich, Zurich, Switzerland

C. AMSler⁸, K. Bösiger, L. Caminada, F. Canelli, V. Chiochia, A. de Cosa, C. Galloni, T. Hreus, B. Kilminster, C. Lange, R. Maier, J. Ngadiuba, D. Pinna, P. Robmann, S. Taroni, Y. Yang

Paul Scherrer Institut, Villigen, Switzerland

W. Bertl, K. Deiters, W. Erdmann, R. Horisberger, H.-C. Kaestli, D. Kotlinski, U. Langenegger, B. Meier, T. Rohe, S. Streuli

National Taiwan University (NTU), Taipei, Taiwan

P.-H. Chen, C. Dietz, U. Grundler, W.-S. Hou, R.-S. Lu, M. Moya

University of Bristol, Bristol, UK

D. Cussans, H. Flacher, J. Goldstein, M. Grimes, J. Jacob, S. Seif El Nasr-Storey

Brunel University, Uxbridge, UK

J. Cole, C. Hoad, P. Hobson, A. Morton, I. D. Reid

Imperial College, London, UK

G. Auzinger, R. Bainbridge, P. Dauncey, G. Hall, T. James, A.-M. Magnan, M. Pesaresi, D. M. Raymond, K. Uchida

Rutherford Appleton Laboratory, Didcot, UK

J. A. Coughlan, K. Harder, J. Ilic, I. R. Tomalin

Brown University, Providence, USA

A. Garabedian, U. Heintz, M. Narain, J. Nelson, S. Sagir, T. Speer, J. Swanson, D. Tersegno, J. Watson-Daniels

University of California, Davis, Davis, USA

M. Chertok, J. Conway, R. Conway, C. Flores, R. Lander, D. Pellett, F. Ricci-Tam, M. Squires, J. Thomson, R. Yohay

University of California, Riverside, Riverside, USA

K. Burt, J. Ellison, G. Hanson, M. Olmedo, W. Si, B. R. Yates

University of California, San Diego, La Jolla, USA

R. Gerosa, V. Sharma, A. Vartak, A. Yagil, G. Zevi Della Porta

Department of Physics, University of California, Santa Barbara, Santa Barbara, USA

V. Dutta, L. Gouskos, J. Incandela, S. Kyre, S. Mullin, A. Patterson, H. Qu, D. White

The Catholic University of America, Washington, DC, USA

A. Dominguez, R. Bartek

University of Colorado Boulder, Boulder, USA

J. P. Cumalat, W. T. Ford, F. Jensen, A. Johnson, M. Krohn, S. Leontsinis, T. Mulholland, K. Stenson, S. R. Wagner

Fermi National Accelerator Laboratory, Batavia, USA

A. Apresyan, G. Bolla[†], K. Burkett, J. N. Butler, A. Canepa, H. W. K. Cheung, J. Chramowicz, D. Christian, W. E. Cooper, G. Deptuch, G. Derylo, C. Gingu, S. Grünendahl, S. Hasegawa, J. Hoff, J. Howell, M. Hrycyk, S. Jindariani, M. Johnson, F. Kahlid, C. M. Lei, R. Lipton, R. Lopes De Sá, T. Liu, S. Los, M. Matulik, P. Merkel, S. Nahn, A. Prosser, R. Rivera, B. Schneider, G. Sellberg, A. Shenai, L. Spiegel, N. Tran, L. Uplegger, E. Voirin

University of Illinois at Chicago (UIC), Chicago, USA

D. R. Berry, X. Chen, L. Ennesser, A. Evdokimov, O. Evdokimov, C. E. Gerber, D. J. Hofman, S. Makauda, C. Mills, I. D. Sandoval Gonzalez

The Ohio State University, Columbus, USA

J. Alimena, L. J. Antonelli, B. Francis, A. Hart, C. S. Hill

Purdue University Calumet, Hammond, USA

N. Parashar, J. Stupak

Purdue University, West Lafayette, USA

D. Bortoletto, M. Bubna, N. Hinton, M. Jones, D. H. Miller, X. Shi

The University of Iowa, Iowa City, USA

P. Tan

The University of Kansas, Lawrence, USA

P. Baringer, A. Bean, S. Khalil, A. Kropivnitskaya, D. Majumder, G. Wilson

Kansas State University, Manhattan, USA

A. Ivanov, R. Mendis, T. Mitchell, N. Skhirtladze, R. Taylor

Johns Hopkins University, Baltimore, USA

I. Anderson, D. Fehling, A. Gritsan, P. Maksimovic, C. Martin, K. Nash, M. Osherson, M. Swartz, M. Xiao

University of Mississippi, Oxford, USA

J. G. Acosta, L. M. Cremaldi, S. Oliveros, L. Perera, D. Summers

University of Nebraska-Lincoln, Lincoln, USA

K. Bloom, D. R. Claes, C. Fangmeier, R. Gonzalez Suarez, J. Monroy, J. Siado

Northwestern University, Evanston, USA

K. Hahn, S. Sevova, K. Sung, M. Trovato

Rutgers, The State University of New Jersey, Piscataway, USA

E. Bartz, Y. Gershtein, E. Halkiadakis, S. Kyriacou, A. Lath, K. Nash, M. Osherson, S. Schnetzer, R. Stone, M. Walker

University of Puerto Rico, Mayaguez, USA

S. Malik, S. Norberg, J. E. Ramirez Vargas

State University of New York at Buffalo, Buffalo, USA

M. Alyari, J. Dolen, A. Godshalk, C. Harrington, I. Iashvili, A. Kharchilava, D. Nguyen, A. Parker, S. Rappoccio, B. Roozbahani

Cornell University, Ithaca, USA

J. Alexander, J. Chaves, J. Chu, S. Dittmer, K. McDermott, N. Mirman, A. Rinkevicius, A. Ryd, E. Salvati, L. Skinnari, L. Soffi, Z. Tao, J. Thom, J. Tucker, M. Zientek

Rice University, Houston, USA

B. Akgün, K. M. Ecklund, M. Kilpatrick, T. Nussbaum, J. Zabel

University of Rochester, Rochester, USA

B. Betchart, R. Covarelli, R. Demina, O. Hindrichs, G. Petrillo

Texas A&M University, College Station, USA

R. Eusebi, I. Osipenkov, A. Perloff, K. A. Ulmer

Vanderbilt University, Nashville, USA

A. G. Delannoy, P. D'Angelo, W. Johns

† Deceased

- 1: Also at Vienna University of Technology, Vienna, Austria
- 2: Also at Université de Haute-Alsace, Mulhouse, France
- 3: Also at Brandenburg University of Technology, Cottbus, Germany
- 4: Also at Horia Hulubei National Institute of Physics and Nuclear Engineering (IFIN-HH), Bucharest, Romania
- 5: Also at Università degli Studi di Siena, Siena, Italy
- 6: Also at CNRS-IN2P3, Paris, France
- 7: Also at Institute for Theoretical and Experimental Physics, Moscow, Russia
- 8: Also at Albert Einstein Center for Fundamental Physics, Bern, Switzerland